Ionics
https://doi.org/10.1007/s11581-024-05724-w

RESEARCH

Co-free and Sr-free double-perovskite oxide $PrBaFe_{1.9}Nb_{0.1}O_{5+\delta}$ as a potential electrode material for symmetrical solid oxide fuel cells

Feng Wang[1] · Jinyan Qi[1] · Pengkai Shan[1] · Bin Qian[1] · Lishuai Xie[2] · Yifeng Zheng[1] · Han Chen[1] · Lin Ge[1]

Received: 19 February 2024 / Revised: 27 June 2024 / Accepted: 16 July 2024

Abstract

Double-perovskite oxide $PrBaFe_2O_{5+\delta}$ (PBF) is considered as a potential electrode material because of its superior oxygen reduction reaction (ORR) activity in air and excellent stability in wet hydrogen atmospheres. However, the electrochemical activities of Fe-based electrode materials are constrained by the oxygen vacancy concentration and oxy-ion transport properties. Herein, $PrBaFe_{2-x}Nb_xO_{5+\delta}$ (PBFNx, $x = 0$, 0.05, 0.1, 0.15) oxides are synthesized and evaluated as electrodes for symmetrical solid oxide fuel cell (SSOFC). X-ray diffraction (XRD) indicates that PBFNx samples have an orthorhombic structure and good chemical compatibility with electrolyte. Among all the samples, the PBFN0.1 symmetrical half-cell shows the lowest polarization resistance at 800 °C, which decreases by 29.2% compared with that of PBF in air and decreases by 59.9% compared with that of PBF in wet hydrogen atmospheres. The output performance of the single cell with PBFN0.1 as symmetrical electrodes achieves 197.10 mW cm^{-2} in wet hydrogen atmospheres at 800 °C, which is an improvement of 31.97% compared with that of PBF. The enhanced electrochemical performance can be attributed to an increase in oxygen vacancy concentrations. The results suggest that the PBFN0.1 material is a potential candidate for SSOFC.

Keywords Symmetrical solid oxide fuel cells · Double perovskite · Nb doping · Electrochemical performance

Introduction

Solid oxide fuel cell (SOFC) is a high-efficiency energy conversion device that can directly convert chemical energy in various fuels into electrical energy. Considering its excellent fuel flexibility, high efficiency, and environmental friendliness, SOFC has shown great application potential in the electrochemical field [1–3]. A conventional SOFC configuration consists of three components, namely, porous anode, dense electrolyte, and porous cathode, and the electrodes normally use different materials because they are exposed to different working environments [4–6]. In recent years, symmetrical SOFC (SSOFC) with the new configuration of the A | B | A structure, where the cathode and anode use the same electrode material, has attracted significant attention. The preparation process can be greatly simplified to decrease the cost for operating and maintenance, thereby minimizing compatibility problems and improving thermal and long-term operational stability. Furthermore, this cell configuration eliminates carbon deposition and sulfur poisoning by switching the direction of gas flow [7–11]. However, the performance of SSOFC is limited by the electrodes. For SSOFC to work well, the electrode materials of the SSOFC require good structural and chemical stability in oxidizing and reducing atmospheres as well as excellent electrocatalytic activity for the oxygen reduction reaction (ORR) and hydrogen oxidation reaction (HOR) [12–14]. Recently, single-perovskite oxides (ABO_3 type) and double-perovskite oxides ($AA'BO_{5+\delta}$ or $AA'B'B''O_{6-\delta}$ type) are primarily used as electrode materials for SSOFC [15], including Mn-, Cr-, Sr-, Fe-, and Co-based oxides [16]. Although Sr- and Co-based oxides show excellent catalytic activity and high electrical conductivity, they also encounter some issues. Co-based perovskite materials may suffer some problems, including poor stability and relatively high price of cobalt element [17]. Sr cations often show surface segregation or secondary phases with critical impurities

✉ Yifeng Zheng
zhengyifeng@njtech.edu.cn

[1] College of Materials Science and Engineering, Nanjing Tech University, No. 30 South Puzhu Road, Nanjing 211816, Jiangsu, China

[2] Jiangsu Key Laboratory of Advanced Structural Materials and Application Technology, Nanjing Institute of Technology, Nanjing 211167, China

Published online: 27 July 2024

[18]. Several recent studies have shown that Co-free and Sr-free layered perovskite oxides may be suitable candidates, which can overcome these complex shortcomings. In particular, Fe-based perovskites have attracted considerable interest due to their good catalytic activity [19], low cost of iron, and suitable TEC, such as single-perovskite oxides ($SrFeO_3$ and $BaFeO_3$) [20] and double-perovskite oxides ($Sr_2Fe_{1.5}Mo_{0.5}O_{6-\delta}$ and $LnBaFe_2O_{5+\delta}$ [LnBFO, Ln = La, Pr, Sm, and Gd]) [21, 22].

In the $LnBaFe_2O_{5+\delta}$ series, $PrBaFe_2O_{5+\delta}$ (PBF) oxides have been reported as electrode materials for SSOFC because of their rapid oxygen ion diffusion, excellent ORR activity, and superior stability in H_2 atmospheres [23]. The $PrBaFe_2O_{5+\delta}$ sample with symmetrical electrodes exhibits superior redox stability and high peak power density (PPD). The stability has been investigated, and the $PrBaFe_2O_{5+\delta}$ shows excellent chemical stability in CO_2 atmosphere [24, 25]. Compared with Co-based perovskite materials, the electrochemical activity of Fe-based perovskites lags behind a long distance. For example, at 700 °C, the interfacial polarization resistance of $LaBaFe_2O_{5+\delta}$ is 1.12 Ω cm^2, approximately 3 times higher than the value of $LaBaCo_2O_{5+\delta}$, which can be attributed to higher energy barriers for the formation of oxygen vacancies and diffusion of oxygen ions [26]. Therefore, the electrochemical catalytic activity still needs to be further improved. Based on literature, b-site cations and oxygen vacancies may be the main factors influencing electrochemical catalytic activity [27, 28]. As is known to all, elemental doping is an effective method for improving the electrochemical activity [29, 30]. $PrBa(Fe_{0.8}Sc_{0.2})_2O_{5+\delta}$ was prepared and applied as symmetrical electrodes for SSOFC, and the Sc-doped electrode showed low polarization resistance (Rp) of 0.18 Ω·cm^2 in wet H_2 [31]. W-doped $PrBaFe_2O_{5+\delta}$ greatly improves the electrochemical performance and maintains excellent stability in air and hydrogen atmospheres [23]. Mo-doped $PrBaFe_2O_{5+\delta}$ has shown higher power density than the parent phase PBF [32]. In our previous work, Ta-doped $PrBaFe_2O_{5+\delta}$ perovskite achieved the Rp of 0.171 and 0.503 Ω cm^2 in air and H_2 at 800 °C, respectively [33].

Nb is an effective dopant for the B-site of perovskite oxides, which can significantly enhance their structural stability and constrain the oxidation state changes of other ions on the B-site due to the formation of strong Nb-O bond [34, 35]. In addition, the ionic radius of Nb^{5+} (0.064 nm) is very close to that of Fe^{3+} (0.0645 nm), making it easier for Nb ions to partially replace Fe ions on the B-site [36]. The performance of the Nb-doped $LaBaFe_{2-x}Nb_xO_{6-\delta}$ cathode has been evaluated, and the electrochemical performance and electrocatalytic activity were significantly improved by Nb-doped [37]. In addition, perovskite $La_{0.6}Sr_{0.4}Fe_{1-x}Nb_xO_{3-\delta}$ oxides as fuel electrodes have been investigated in our previous study. Nb doping can improve the electrochemical catalytic activity in CO_2 atmospheres [38]. However, few studies have been conducted on Nb-doped $PrBaFe_2O_{5+\delta}$ as the symmetrical electrode of SSOFC.

In this paper, Nb-doped $PrBaFe_2O_{5+\delta}$ (PBFNx, x = 0, 0.05, 0.1, 0.15) oxides were synthesized and analyzed as symmetrical electrodes of SSOFC. The effect of Nb-doped PBF on the crystal structure, conductivity, electrochemical performance, and output performance was also investigated.

Experimental

Preparation of materials

The powders of $PrBaFe_{2-x}Nb_xO_{5+\delta}$ (PBFNx, x = 0, 0.05, 0.1, 0.15) were synthesized via a conventional solid-state reaction method. Stoichiometric amounts of Pr_6O_{11} (99.99%, Shanghai Macklin Biochemical Co., Ltd.), $BaCO_3$ (99.99%, Sinopharm Chemical Reagent Co., Ltd.), Fe_2O_3 (99.99%, Sinopharm Chemical Reagent Co., Ltd.), and Nb_2O_5 (99.99%, Sinopharm Chemical Reagent Co., Ltd.) powders were fully mixed and then homogenized in ethanol by ball milling for 24 h. After drying the milled solutions, the obtained powders were then calcined at 1200 °C for 6 h. The resultant oxides were grounded and dried using the abovementioned method and then passed through a sieve (80 mesh). Subsequently, the powders were pressed into pellets or rectangular bars using a cuboid mold and sintered at 1350 °C for 5 h. GDC ($Gd_{0.1}Ce_{0.9}O_{2-\delta}$) and YSZ (yttria-stabilized zirconia) powders were bought from Ningbo SOFCMAN Energy Technology Co., Ltd., China.

Material characterization

X-ray diffraction (XRD, Empyrean, PANalytical, The Netherlands) with Cu-Ka radiation accurately analyzed the crystal structure of all samples. A scanning speed of 10° per minute was used in the diffraction angle range of 20–80° at room temperature. X-ray photoelectron spectroscopy (XPS, Thermo Scientific K-Alpha) was utilized to assess the composition and chemical elemental state of Fe2p and O1s ions in the PBFNx samples. The microstructure of the PBFN0.1|GDC|YSZ|GDC|PBFN0.1 symmetrical cell was observed by scanning electron microscopy (SEM, JSM-7600F, JEOL, Japan). For the electrical conductivity, the PBFNx sample materials were measured in air and humidified H_2 by using a four-probe direct DC method equipped with a Keithley 2420 source meter with a temperature range of 300–800 °C and under an atmosphere with $p(O_2)$ = 0.21 atm.

Cell fabrication and electrochemical performance

The Rp of half cells (with the configuration of PBFNx|GDC|PBFNx in air or PBFNx|GDC|YSZ|GDC|PBFNx in H_2) was measured using the CHI660e workstation with a frequency range of 10^6 to 0.1 Hz from 600 to 800 °C in a step of 50 °C. Furthermore, half cells with the configuration of PBFNx|GDC|PBFNx ($x = 0$, 0.1) were used to study the ORR kinetics of the PBF and PBFN0.1 electrodes at 800 °C. The electrolyte-supported single cells with the configuration of PBFNx|GDC|YSZ|GDC|PBFNx were fabricated to obtain the current density versus the voltage (I–V) and current density versus power output (I–P) curves. A half cell was prepared with a 0.5-mm-thick GDC electrolyte, and a full cell was prepared with a 0.3 mm-thick YSZ electrolyte. First, the YSZ electrolyte powders were ground and shaped into disk-shaped pellets at 100 MPa using a 18-mm-diameter cylindrical stainless-steel die. Then, the pellets were sintered at 1450 °C for 5 h in air to obtain dense pellets. The GDC slurry was deposited onto both sides of the YSZ by using a conventional screen-printing technique and was subsequently sintered at 1300 °C for 2 h. The as-prepared electrode slurry was painted on both sides of the GDC interlayer and sintered at 1000 °C in air for 2 h to form symmetrical cells. The electrode has an active area of 0.5 cm^2. The single cells were assembled and sealed on the top of an alumina tube using a conductive resin (DAD-87, Shanghai Research Institute of Synthetic Resins) as sealant. The electrochemical performance of the single cell was measured using an electrochemical workstation (CHI660e) at a temperature range of 600–800 °C with humidified hydrogen (~3% H_2O) as the fuel and ambient air as the oxidant. The flow rate of humidified hydrogen was 50 mL·min^{-1}. After measuring the single cell, the short-term stability of the symmetrical cell with the PBFN0.1 electrode was evaluated in humidified hydrogen atmospheres by using the same electrochemical workstation.

Results and discussion

Crystal structure

Figure 1a shows the XRD patterns of the as-prepared PBFNx ($x = 0$, 0.05, 0.1, 0.15) powders calcined at 1200 °C for 6 h in air. PBFNx materials are an orthorhombic double-perovskite structure (space group: Pmmm) with no impurity phases, indicating that Nb element has been successfully doped into the PBF powder, and it is consistent with that of the $PrBaFe_2O_{5+\delta}$ materials in the previous study [39]. In addition, as shown in the enlarged view of the (110) peak of PBFNx (Fig. 1b), Nb doping slightly shifts the diffraction peaks of PBF to a lower angle, which can be attributed to the fact that the radius of Nb^{5+} (0.70 Å) is larger than that of Fe^{3+} (0.65 Å)/Fe^{4+} (0.59 A°) [38]. In obtaining structural information of PBFNx samples, Rietveld refinements of XRD data are shown in Fig. 1c–f, and Table 1 shows the detailed refinement results. The lattice parameters of the parent PBF powder are $a = 3.9351$ Å, $b = 3.9364$ Å, and $c = 7.8514$ Å, which are close to the results reported by Lü et al. [40]. Doping Nb slightly increases the lattice volume from 121.81 to 123.60 $Å^3$. The lattice parameter of the PBFN0.1 powder is a =3.9571 Å, b =3.9460 Å, and $c = 7.8752$ Å.

Chemical and thermal compatibility

Good chemical compatibility between electrode and electrolyte is important to the application of SSOFC [41]. Therefore, to evaluate the chemical compatibility between electrode and electrolyte materials, the electrode materials were sintered at 1000 °C for 2 h with a 1:1 mass ratio of GDC or YSZ electrolytes (Fig. 2). Figure 2a shows that new diffraction peaks were observed, indicating the formation of new phases. Consequently, the YSZ electrolyte has poor compatibility with PBFNx electrodes, and this electrolyte cannot be used directly as the support electrolyte material. Figure 2b shows no any new diffraction peaks and shifts, indicating that PBFN0.1 has good chemical compatibility with the GDC electrolyte. Thus, GDC can be used as an electrolyte for symmetrical cells or as a buffer layer to prevent the reaction between the electrolyte and electrode.

XPS analysis

XPS can be utilized to analyze the composition and surface chemical states of Fe2p and O1s ions for the PBFNx samples in the air. Figure 3a displays the high-resolution XPS spectra of Fe2p in the PBFNx samples. The fitting peaks located at ~709.9 /723.5 eV and ~711.8/725.0 eV can represent Fe^{3+} and Fe^{4+} ions, respectively. Furthermore, the satellite peak at ~717.7 eV is assigned to the Fe^{3+} species [42]. In Table 2, with the increase of Nb substitution, the ratios of Fe^{4+}/Fe^{3+} induce an obvious decline, implying the reduction of Fe ions from Fe^{4+} to Fe^{3+} ($2Fe_{Fe}^{\bullet} + O_O^X \iff 2Fe_{Fe}^X + V_o^{\bullet\bullet} + \frac{1}{2}O_2$) to achieve electrical neutrality and the formation of more oxygen vacancies [37]. The increase of Fe^{3+} and oxygen vacancies results in the expanding lattice, which is consistent with the XRD result (Fig. 1b). As depicted in Fig. 3b, it was observed that the two fitting peaks in the spectra are lattice oxygen and absorbed oxygen. The lattice oxygen peak is located at ~528.5 eV, while the absorbed oxygen peak is located at ~531.3 eV [43]. One criterion for evaluating the relative content of oxygen vacancy in materials is the ratio of O_{ads}/O_{lat} [44]. The O_{ads}/O_{lat} values are 1.29, 1.94, 1.77, and 1.5 for PBFNx at $x = 0$, 0.05, 0.1, and 0.15, respectively, suggesting the formation of more oxygen vacancies after Nb doping. For PBFNx ($x = 0.05$, 0.1,

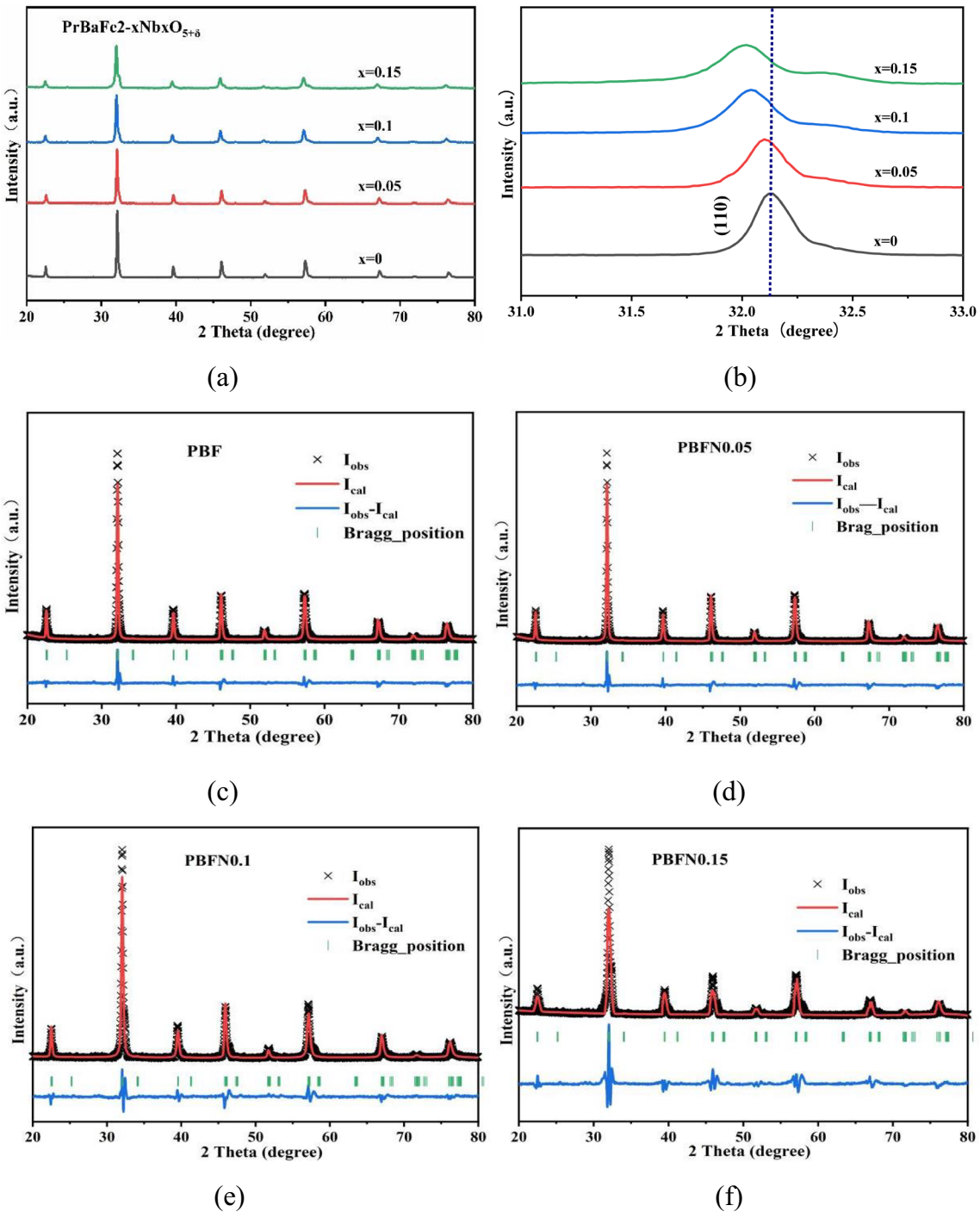

Fig. 1 **a** XRD patterns of PBFNx (x = 0, 0.05, 0.1, 0.15), **b** enlarged view of 31° to 33°. Rietveld refined powder XRD patterns of **c** PBF, **d** PBFN0.05, **e** PBFN0.1, and **f** PBFN0.15

Table 1 XRD Rietveld refinement results of PBFNx (x = 0, 0.05, 0.1, 0.15) oxides

Sample	a (Å)	b (Å)	c (Å)	V (Å^3)	R_p	R_{wp}
$x = 0$	3.9351	3.9364	7.8514	121.81	6.01	8.22
$x = 0.05$	3.9496	3.9407	7.8598	122.33	6.88	9.38
$x = 0.1$	3.9571	3.9460	7.8752	122.96	6.68	9.31
$x = 0.15$	3.9681	3.9544	7.8769	123.60	10.17	14.44

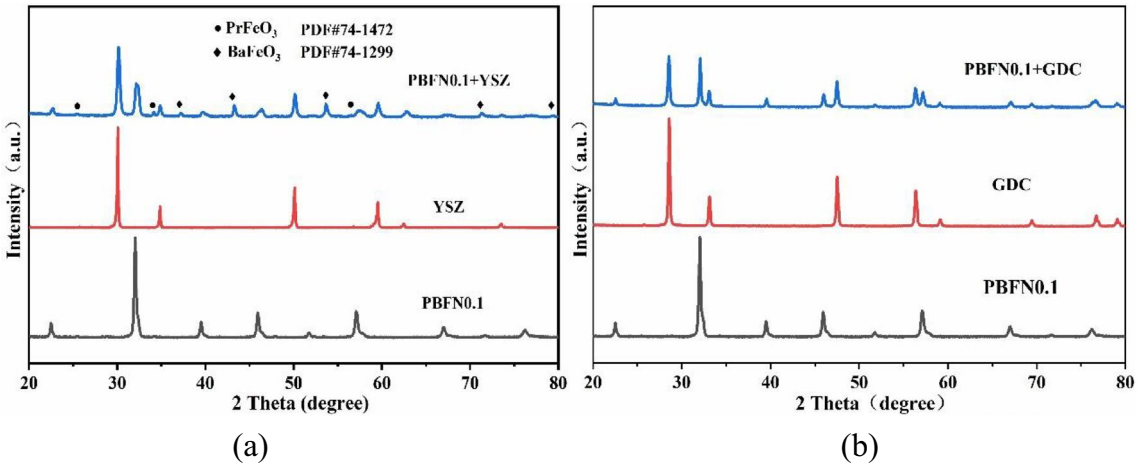

Fig. 2 XRD patterns of **a** PBFO + YSZ and **b** PBFNO + GDC mixtures

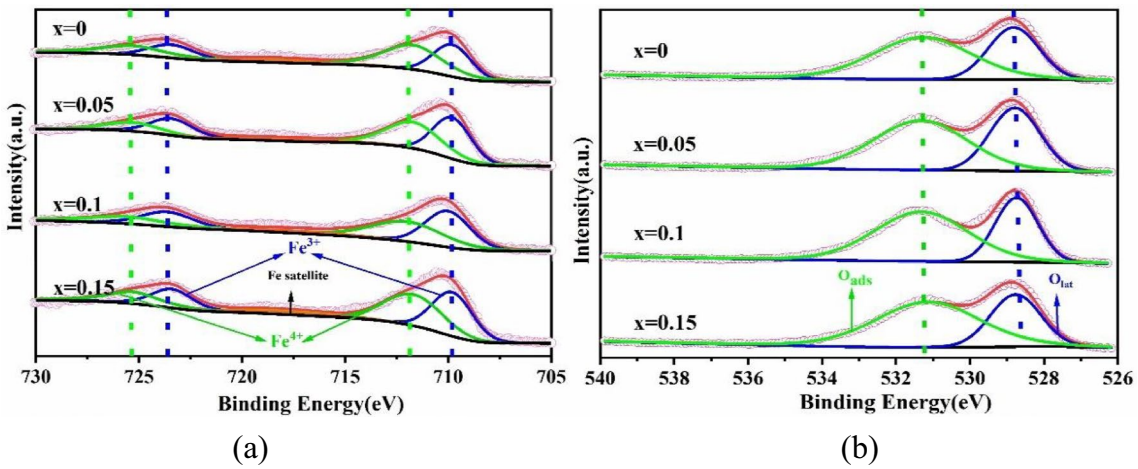

Fig. 3 XPS spectra of the PBFNx: **a** Fe2p and **b** O1s

Table 2 Fitting data of Fe2p and O1s for PBFNx powders

Sample	Fe2p (%)			O1s (%)		
	Fe^{4+}	Fe^{3+}	Fe^{4+}/Fe^{3+}	O_{ads}	O_{lat}	O_{ads}/O_{lat}
PBF	60%	40%	1.50	62%	48%	1.29
PBFN0.05	49%	51%	0.96	66%	34%	1.94
PBFN0.1	39%	61%	0.64	64%	36%	1.77
PBFN0.15	34%	66%	0.51	60%	40%	1.5

0.15) oxides, the oxygen vacancies exhibit a downward trend with increasing the amount of Nb doping, which is attributed to the stronger ionic affinity of Nb with O than of Fe. Based on literature, oxygen vacancies are important for the transport of oxygen ions during the oxygen reduction reaction (ORR) [45]. Consequently, the XPS results show that the Nb doping of PBF samples is beneficial for achieving good electrochemical performance.

Electrical conductivity

For mixed ionic–electronic conductor materials, electron conduction and ion conduction exist simultaneously. However, electronic conductivity is usually at least two orders of magnitude higher than ion conductivity, so the conductivity primarily refers to the electronic conductivity [46]. Figure 4a shows the conductivity of PBFNx (x = 0, 0.05, 0.1, 0.15)

at different temperatures, ranging from 300 to 800 °C in the air. At below 450 °C, the conductivity of each composition in PBFNx increases because of the existence of a small polaron hopping conduction mechanism, indicating a semiconductor-like behavior. At about 450 °C in air, the conductivities of PBFNx reach maximum values. With the further increase in temperature, the oxygen lattice may lose along with the generation of oxygen vacancies and a mobility barrier of electronic conduction carriers. Consequently, the conductivity drops and shows a metallic-like behavior [47]. With increasing the amount of Nb doping, the conductivity exhibits a downward trend, which is ascribed to the increase in non-conducting Nb-O bonds and the decrease in the concentration of Fe^{4+}. For further study, the conductivity of PBFNx ($x = 0, 0.05, 0.1, 0.15$) is measured in hydrogen. As shown in Fig. 4b, the conductivity of all samples increases with the increase of temperature. However, the electrical conductivity of PBFNx samples in H_2 is lower than that of samples in air because of the presence of reduction reactions. Zhao et al. reported that $Fe^{\cdot}_{Fe}(Fe^{4+}/Fe^{3+})$ are the mobile electronic holes, providing a significant contribution to electronic conduction. Under reducing conditions, electronic holes in PBFNx would reduce, leading to a decrease in electrical conductivity (A novel layered perovskite as symmetrical electrode for direct hydrocarbon solid oxide fuel cells). Furthermore, appropriate amount of Nb doping improves the conductivity of PBF in H_2 atmosphere, which is attributed to the high-valence Nb^{5+} replacing Fe^{4+} and Fe^{3+} and promoting the concentration of free electrons [48]. The maximum conductivity of PBFNx samples is 46.35 S cm^{-1} in air and 3.74 S cm^{-1} in H_2, which is higher than that of symmetrical electrodes, such as $SrFe_{0.8}W_{0.2}O_3$ (1.16 S cm^{-1} in H_2) [49], $La_{0.5}Sr_{0.5}Fe_{0.9}Nb_{0.1}O_{3-\delta}$ (0.47 S cm^{-1} in H_2) [48], and $Sr_2TiFe_{0.9}Mo_{0.1}O_6$ (0.90 and 0.26 S·cm^{-1} in air and H_2) [50].

Half-cell performance

To study the electrochemical performance of PBFNx ($x = 0, 0.05, 0.1, 0.15$) symmetrical electrodes, the impedance of the electrodes was performed on the cells with the configuration of PBFNx|GDC|PBFNx in air at 600–800 °C. The corresponding EIS results were obtained by using Z-view fitting. The impedance of the electrodes primarily contains ohmic resistance (Ro) and polarization resistance (Rp). Ro is defined as the intercept of the semicircle on the real axis, including GDC electrolyte, PBFNx electrodes, and other contact resistance [51]. Rp is defined as the distance between semicircles on the real axis, which is primarily due to charge transfer, surface adsorption, and oxygen diffusion, and is an essential index to determine the electrochemical catalytic activity of SSOFC electrodes [52]. For the convenience of comparison, Ro is usually normalized to zero for clarity, and the intersection of two semi-circular arcs and the x axis is the polarization resistance. As shown in Fig. 5a, the Rp value decreases significantly after Nb doping, indicating that the ORR process has been improved. The Rp value of PBFN0.1 is 0.109 Ω cm^2 at 800 °C, which decreases by 29.2% compared with that of PBF. The Rp consists of high-frequency resistance ($R_{HF,}$ >10^3 Hz) and low-frequency resistance (R_{LF}, 10^{-1}–10^3 Hz). The R_{HF} response corresponds to the charge transfer among the interface between the electrode and the electrolyte. The R_{LF} response is associated with gas diffusion and gas transformations (adsorption and desorption) [53]. As shown in Fig. 5b, R_{HF} of the PBFN0.1 electrode is decreased by 22.69% to 0.01025 Ω cm^2 at 800 °C, whereas R_{LF} is decreased by 28.09% to 0.09931 Ω cm^2 at 800 °C. The result indicates that Nb doping promotes electrochemical processes of PBF electrode by the increase in gas diffusion and gas transformations. Figure 5c shows the Rp values of PBFNx at different temperatures, ranging from 600 to 800 °C

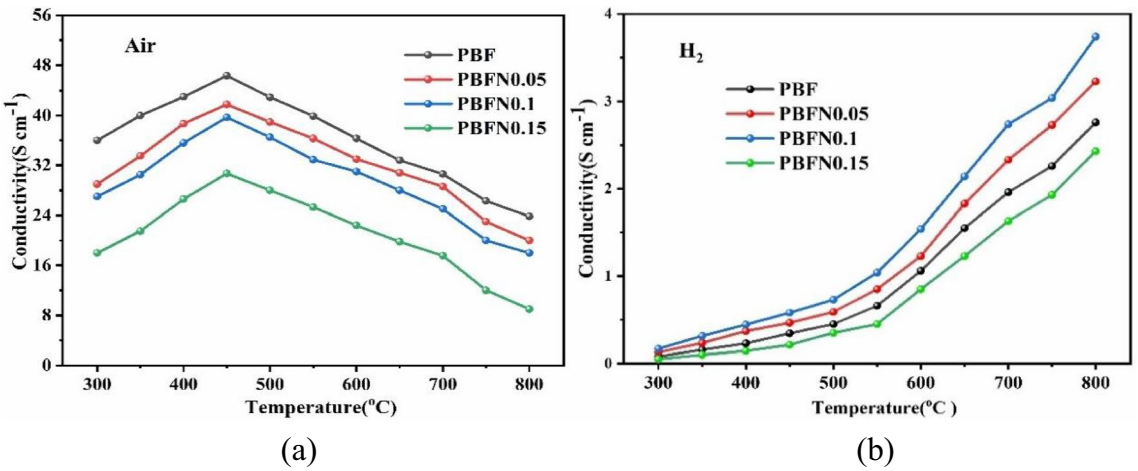

Fig. 4 Conductivity of PBFNx **a** in air and **b** in H_2

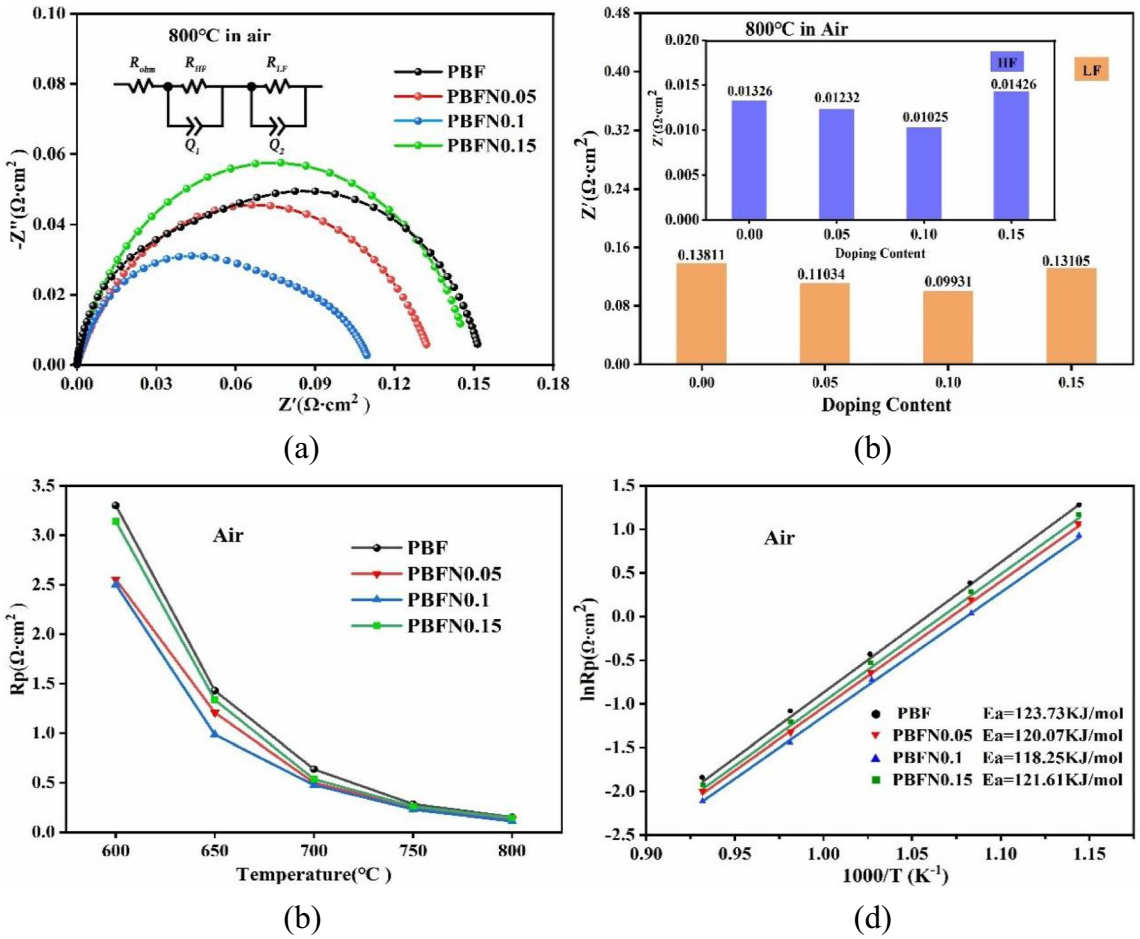

Fig. 5 In air: **a** EIS of PBFNx at 800 °C; **b** Rp of PBFNx at high and low frequencies; **c** Rp of PBFNx at 600–800 °C; **d** Arrhenius plots of PBFNx electrodes

in air. The PBFN0.1 sample obtains the lowest Rp of 2.501, 0.985, 0.476, 0.229, and 0.109 Ω cm^2 at 600 °C, 650 °C, 700 °C, 750 °C, and 800 °C, respectively. Figure 5d shows the Arrhenius curves of Rp of PBFNx electrodes in air. The activation energy (Ea) of the PBFN0.1 electrode is lower than that of PBF, which further indicates that Nb doping improves the catalytic activity of ORR in the PBF electrode.

Based on some GDC literature reports, GDC cannot be used directly as an electrolyte under a hydrogen atmosphere because its structure change (Ce^{4+}→Ce^{3+}) leads to performance degradation [32]. When the YSZ is used as the electrolyte, GDC is required as a buffer layer to prevent reactions between the electrodes and electrolyte (Fig. 2b). The impedance of the electrodes was performed on the cells with the configuration of PBFNx|GDC|YSZ|GDC|PBFNx in hydrogen at 600–800 °C. As shown in Fig. 6a, the Rp value decreases significantly after Nb doping. Among PBFNx electrodes, the $x = 0.1$ sample shows the lowest Rp, which is decreased by 59.9% to 0.391 Ω cm^2 at 800 °C in hydrogen atmospheres. This result indicates that Nb doping can improve the HOR activity. As shown in Fig. 6b, R_{HF} of the PBFN0.1 electrode is decreased by 30.7% to 0.0009 Ω cm^2 at 800 °C, whereas R_{LF} is decreased by 61.33% to 0.3633 Ω cm^2 at 800 °C, suggesting that the HOR is primarily determined by the charge transfer between the electrode and the electrolyte. As shown in Fig. 6c, PBFN0.1 sample has the lowest Rp, which is 6.001, 3.592, 1.877, 0.841, and 0.391 Ω·cm^2 at different temperatures, ranging from 600 to 800 °C in hydrogen atmospheres. As shown in Fig. 6d, the Ea value of the PBFN0.1 electrode is lower than that of the PBF electrode, which further indicates that the introduction of Nb doping into the PBF electrode improves the HOR activity. Based on the abovementioned results, Nb doping can improve the ORR and HOR activity of PBF electrode. In addition, the performance of PBFN0.1 symmetrical electrodes is higher than that of other iron-based perovskite, and the Rp results in the literature are listed in Table 3.

To obtain more insights into the ORR mechanism of electrode, the PBF and PBFN0.1 electrodes with GDC as the electrolyte were measured under different oxygen pressure

Table 3 The polarization resistance of the symmetrical electrodes for symmetrical solid oxide fuel cells

Electrode	Temperature (°C)	Electrolyte	Polarization resistance Ω cm^2		Ref.
			In air	In H_2	
$SmBaMn_{1.9}Mg_{0.1}O_{5+\delta}$	850 °C	LSGM	0.144	0.388	[54]
$La_{0.8}Sr_{0.2}FeO_{3-\delta}$	800 °C	YSZ	0.31	0.58	[55]
$La_{0.8}Sr_{0.2}MnO_{3-\delta}$-GDC	800 °C	YSZ	1.44	5.19	[56]
$CaFe_{0.4}Ti_{0.6}O_{3-\delta}$	800 °C	YSZ	1	1	[57]
PBFN0.1	800 °C	YSZ	0.109	0.391	[This work]

levels at 800 °C, and the EIS data are shown in Fig. 7a, b. Based on literature, the Rp value of the electrodes satisfies a certain relationship with the oxygen partial pressure $p(O_2)$ by using the following expression:

$$\mathrm{Rp} \propto p\left(O_2\right)^{-n} \tag{1}$$

where n represents the number of reaction steps of the electrochemical ORR, satisfying the following correspondence [58, 59]:

$$n = 1,\ O_2(g) \iff O_{2,ads} \tag{2}$$

$$n = 1/2,\ O_{2,ads} \iff 2O_{ads} \tag{3}$$

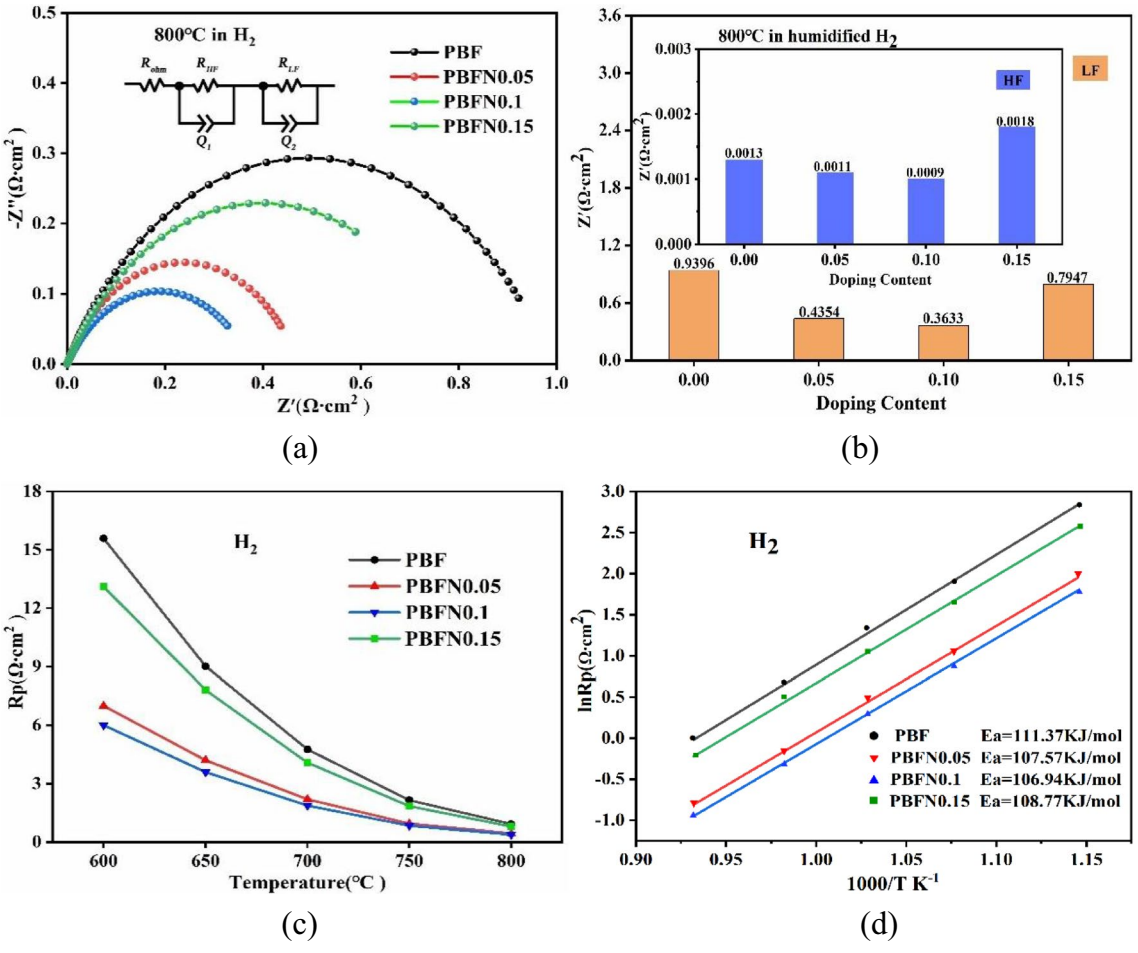

Fig. 6 In H_2: **a** EIS of PBFNx at 800 °C; **b** Rp of PBFNx at high and low frequencies; **c** Rp of PBFNx at 600–800 °C; **d** Arrhenius plots of PBFNx electrodes

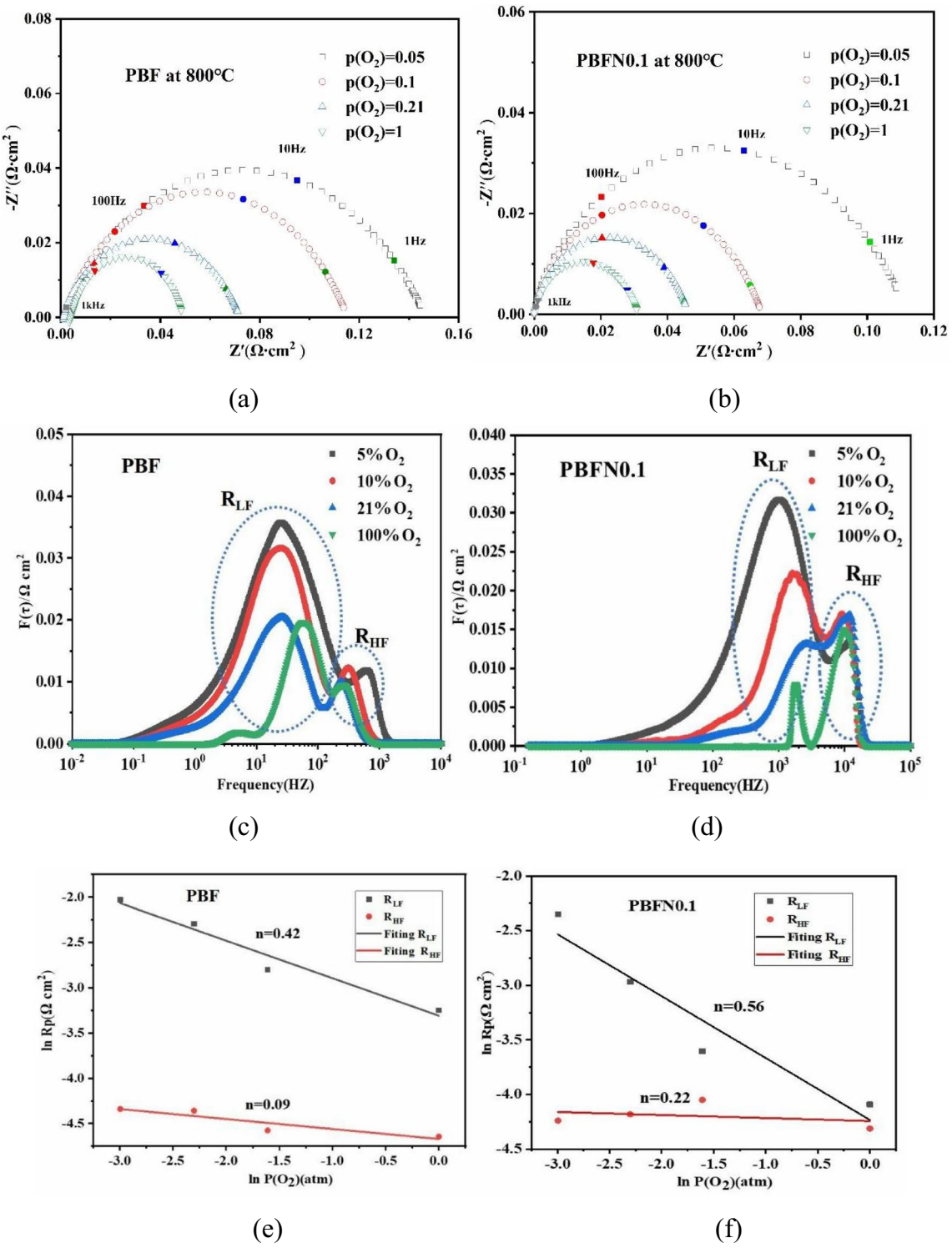

Fig. 7 Polarization resistance of **a** PBF and **b** PBFN0.1 cathodes and various O_2 concentration at 800 °C. DRT curves of **c** PBF and **d** PBFN0.1. **e, f** $p(O_2)$ dependence of Rp for the samples

$$n = 1/4,\ O_{ads} + 2e' + V_o^{\bullet\bullet} \Leftrightarrow O_O^x \quad (4)$$

$$n = 1/10,\ O_{TPB}^{2-} + V_o^{\bullet\bullet} \iff O_O^x \quad (5)$$

The impedance spectrum can be separated into two arcs, namely, R_{HF} and R_{LF}, indicating the rate of ORR reaction consists of two electrochemical processes as illustrated in Fig. 7c, d.

Figure 7e, f takes logarithms of Rp and oxygen partial pressure value $p(O_2)$ to obtain the relationship diagram. The slope of the straight line corresponds to the number of reaction levels n in Eq. (1), where the n value size can be inferred from the reaction steps of the corresponding electrode. As shown in Fig. 7e, the n corresponding to R_{HF} of the PBF electrode is 0.09, which indicates that R_{HF} during the electrode reaction is primarily affected by the transfer of oxygen ions from the double-phase boundaries and triple-phase boundaries reaction to the interior of the electrolyte (Eq. (5)), and the n corresponding to R_{LF} is 0.42, which indicates that R_{LF} is primarily due to the diffusion of adsorbed oxygen on the electrode surface (Eq. (3)). For the PBFN0.1 electrode (Fig. 7f), where the values of n corresponding to R_{HF} and R_{LF} are 0.22 and 0.56, R_{HF} of PBFN0.1 is due to the charge transfer reactions (Eq. (2)), whereas R_{LF} is primarily due to the adsorption and desorption process of oxygen (Eq. (3)). It is observed that R_{LF} is higher than R_{HF} in Table 4, suggesting that the gas diffusion and gas transformation are rate-determining influences for the ORR process. The result is consistent with the EIS analysis.

Single-cell performance

Single cell

To investigate the output performance of PBF and PBFN0.1 symmetrical electrodes in SSOFCs, electrolyte-supported single cells with the configurations of PBF|GDC|YSZ|GDC|PBF and PBFN0.1|GDC|YSZ|GDC|PBFN0.1 were prepared. With humidified hydrogen as fuel and air as an oxidant, the single cell was measured in the temperature range of 600–800 °C. Figure 8a and b shows the I-V and I-P curves of the single cell with PBF and PBFN0.1 as symmetrical electrodes, respectively. As shown in Fig. 8, the open-circuit voltage at 800 ℃ is 1.09 V, which is approximated the theoretical value, indicating that the single cell has good sealing performance and density. At 800 °C, 750 °C, 700 °C, 650 °C, and 600 °C, the PPD of PBF is 134.07, 82.68, 60.64, 32.54, and 15.17 mW cm^{-2}, and the PPD of doped Nb is 197.10, 145.65, 97.38, 60.50, and 31.18 mW cm^{-2}, respectively. The PPD of the electrolyte-supported single cell with PBFN0.1 symmetrical electrodes is higher than that of PBF, indicating that the Nb-doped PBF electrode can effectively promote ORR activity in the electrode. This remarkable improvement was achieved by reducing the Rp of the electrodes. The enhanced output performance of a PBFN0.1 single cell further proves that Nb doping improves the electrochemical performance.

Table 4 The R_{HF} and R_{LF} of the PBFNx (x = 0, 0.1) symmetrical electrodes under various O_2 concentration

	PBF		PBFN0.1	
	R_{HF}	R_{LF}	R_{HF}	R_{LF}
5%	0.01284	0.12945	0.01411	0.09535
10%	0.01262	0.09966	0.01527	0.05136
21%	0.01012	0.05985	0.01743	0.02719
1	0.00852	0.03442	0.0167	0.0134

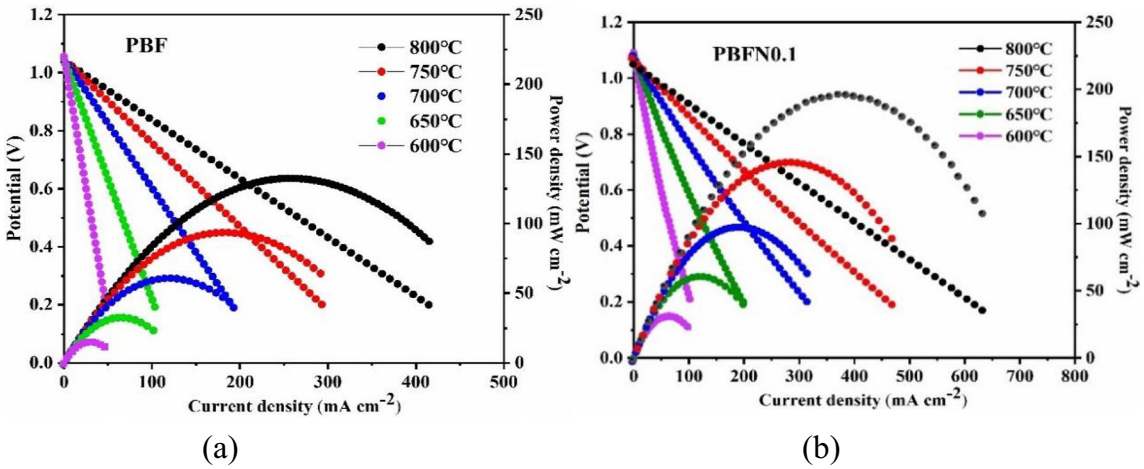

Fig. 8 I-V and I-P curves of **a** PBF and **b** PBFN0.1 as symmetrical electrodes

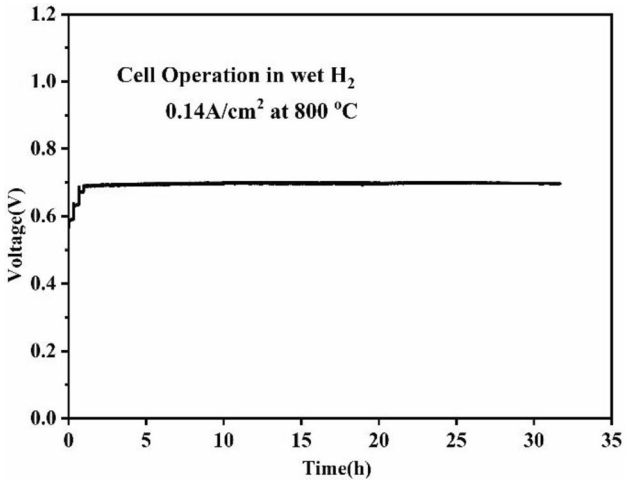

Fig. 9 Stability test of PBFN0.1|GDC|YSZ|GDC|PBFN0.1 operated at 800 °C for 32 h

Stability

Stability is also an important index to evaluate the working state of SSOFC. Therefore, in this experiment, the short-term performance stability of a single cell with PBFN0.1 symmetrical electrodes exposed to 3% H_2O–97% H_2 was maintained at a current density of 0.14 A/cm^2 for 32 h at 800 °C. As shown in Fig. 9, the single cell maintained a relatively stable performance with no degradation under the operating condition, indicating that the PBFN0.1 electrode has good short-term stability.

SEM

Figure 10 shows the morphology of the PBFN0.1|GDC|YSZ|GDC|PBFN0.1 symmetrical cell before and after the stability test at 800 °C. No evident change for electrodes is observed before and after the test. The GDC interlayer is well attached between the porous electrode and the YSZ electrolyte, which promotes the transport of oxygen

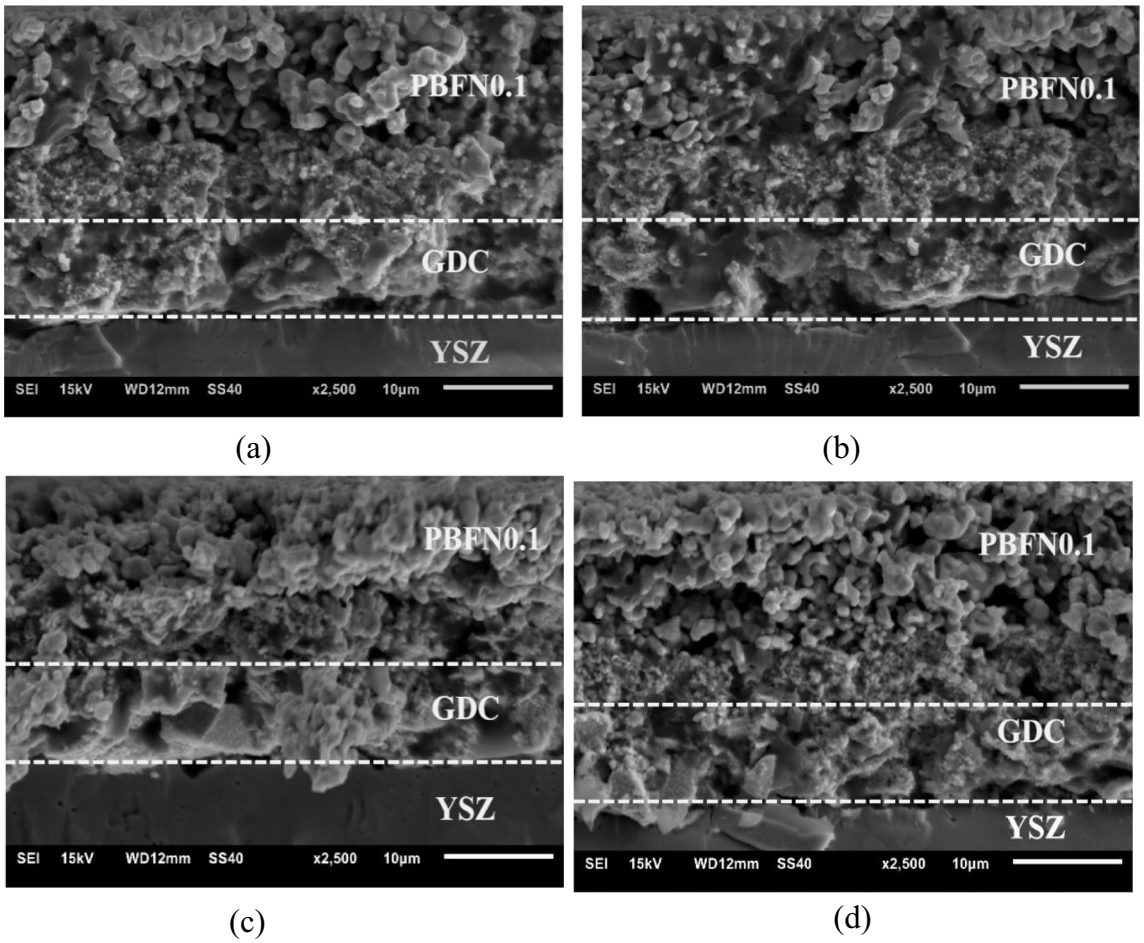

Fig. 10 SEM of PBFN0.1 symmetrical cells. The stability test before: **a** anode and **b** cathode; the stability test after: **c** anode and **d** cathode; EDX element distribution maps of the single cell: **e** anode and **f** cathode

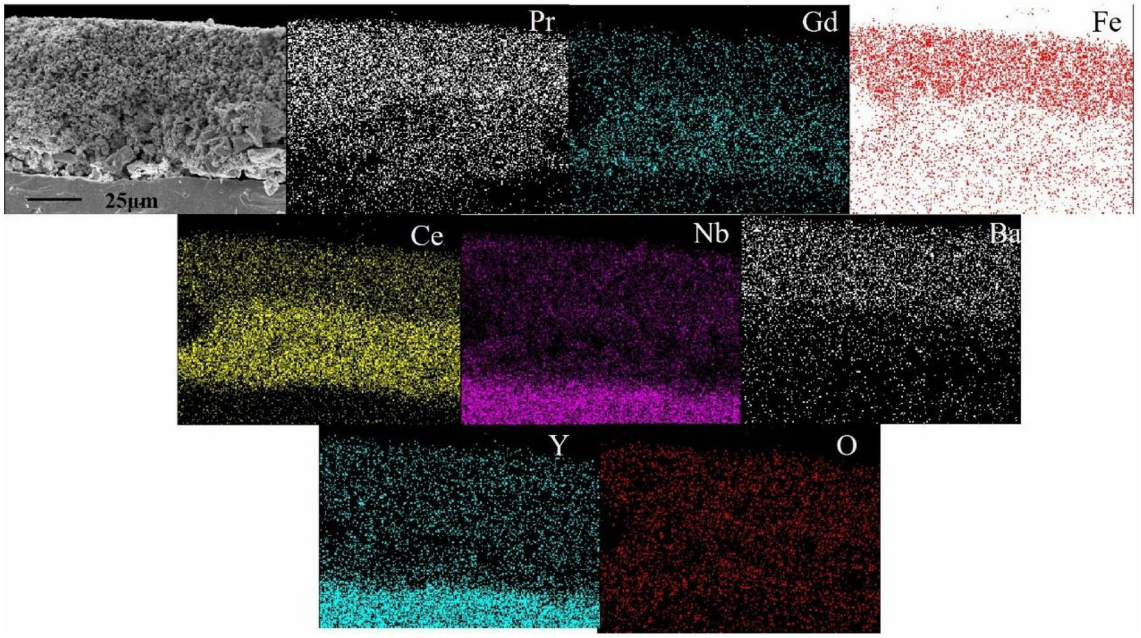

(e)

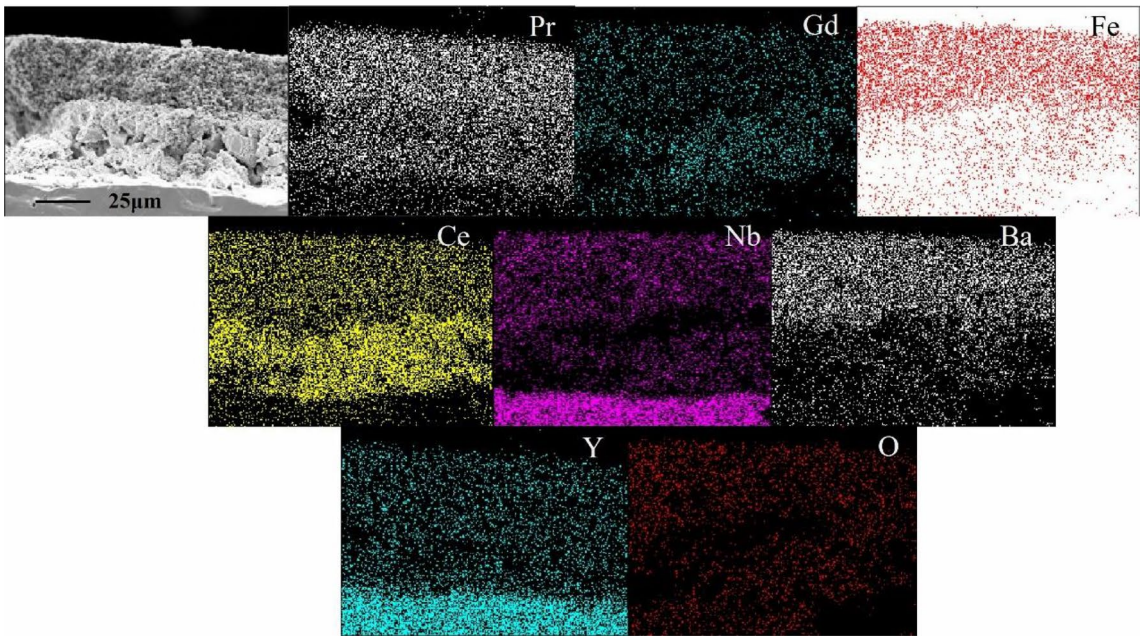

(f)

Fig. 10 (continued)

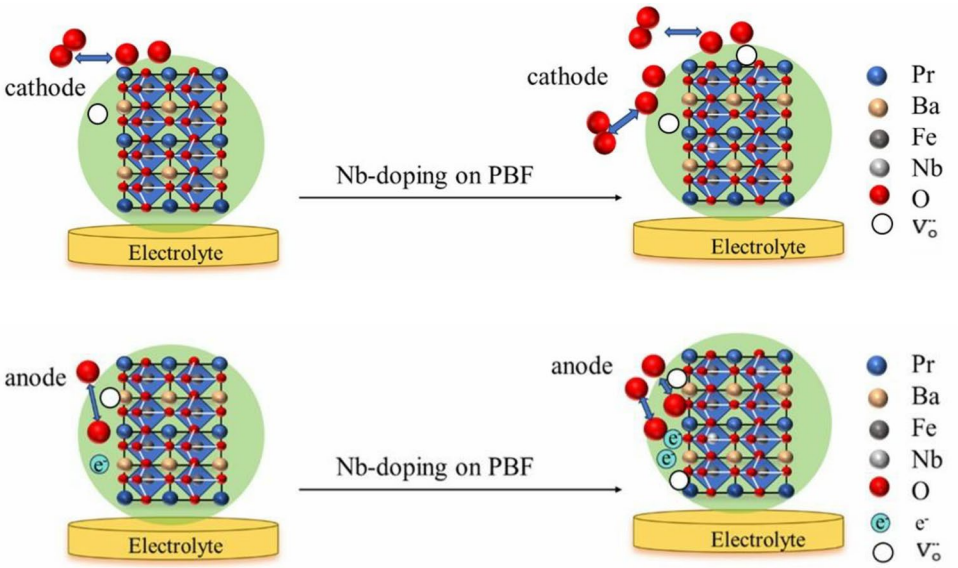

Fig. 11 Schematic of surface adsorption after Nb doping of the cathode (**a**) and anode (**b**)

ions and reduces interfacial resistance. In addition, the electrode region presents a porous structure, which facilitates ion diffusion and transport. The elemental mapping of the single-cell cross-section is shown in Fig. 10e, f, which confirms the presence of Pr, Ba, Fe, Ce, Gd, Zr, Y, Nb, and O elements. In addition, the elements are uniformly distributed as expected. Since the atomic number of Nb is close to that of Zr, the distribution of Nb and Zr elements overlap.

Figure 11 shows the schematic diagram of the cathode and anode after Nb doping. Nb-doped PBF electrodes increase the concentration of oxygen vacancies in air and H_2, which improves the electrochemical catalytic activity of ORR and HOR. However, the mechanism of performance improvement is different. In PBF materials, the oxygen reduction reaction occurs at the cathode, which mainly reduces oxygen and electrons to oxygen ions and transports them to the anode [60]. Doping Nb promotes the adsorption and desorption processes of surface oxygen, which makes it easier for oxygen molecules adsorbed on the surface to be desorbed and enter the interior of the material. This adsorption and desorption process helps to increase the concentration of oxygen vacancies, thereby enhancing the ORR of the material. The function of the anode is to receive electrons from the oxygen ions supplied to the cathode and react with the fuel. Doping Nb promotes electron transport, which leads to the formation of more oxygen vacancies at the anode. Oxygen vacancies could facilitate the increase of the anode surface area for reaction with oxygen, thus improving the electrochemical catalytic activity of HOR (Fig. 11).

Conclusion

Double-perovskite $PrBaFe_{2-x}Nb_xO_{5+\delta}$ (PBFNx, $x = 0$, 0.05, 0.1, 0.15) is synthesized by the solid-state reaction and investigated. The XRD results exhibit that PBFN0.1 shows good chemical compatibility with GDC electrolyte. The XPS results show that Nb doping can increase the concentration of oxygen vacancies and promote oxygen ion transport. In the EIS test, the PBFN0.1 sample shows the lowest Rp values of 0.109 and 0.391 Ω cm^2 in air and H_2, respectively. Furthermore, the PPD of the single cell increases by 31.97% from 134.07 to 197.10 mW cm^{-2}. Moreover, the single cell with the PBFN0.1 cathode exhibits good short-term stability during 32 h after operation. Thus, the novel material PBFN0.1 is a potential candidate electrode for SSOFC.

Author contribution Feng Wang: Conceptualization, Validation, Investigation, Visualization, Formal analysis, Writing - Original Draft. Jinyan Qi: Conceptualization, Investigation, Validation. Pengkai Shan: Conceptualization, Visualization. Bin Qian: Investigation. Lishuai Xie: Validation. Yifeng Zheng: Conceptualization, Resources, Supervision, Writing - Review & Editing. Han Chen: Formal analysis. Lin Ge: Methodology.

Funding This work was supported by the National Natural Science Foundation of China (No. 21978133 and No. 21506100), the Natural Science Foundation of Jiangsu Province (BK 20211260), the Priority Academic Program Development (PAPD) of Jiangsu Higher Education Institutions, and Top-notch Academic Programs Project of Jiangsu Higher Education Institutions (TAPP).

Data availability No datasets were generated or analysed during the current study.

Declarations

Conflict of interest The authors declare no competing interests.

References

1. Li Z, Wan Z et al (2021) A robust network binder via localized linking by small molecules for high-areal-capacity silicon anodes in lithium-ion batteries. Nano Energy 79:105430. https://doi.org/10.1016/j.nanoen.2020.105430
2. Kim J, Rehman SU et al (2023) Vertical-cavity surface-emitting laser (VCSEL)-based ultrafast photonic sintering of solid oxide fuel cells (SOFCs): prospects for time-efficient/two-dimensional scalability to large-sized SOFCs. J Mater Chem A 11(17):9474–9484. https://doi.org/10.1039/d3ta00602f
3. Shah M, Lu YZ et al (2023) Semiconductor-membrane fuel cell (SMFC) for renewable energy technology. Renew Sust Energ Rev 185:24. https://doi.org/10.1016/j.rser.2023.113639
4. Yang Y, Chen ZP et al (2023) A highly efficient bismuth substitution induced A-site ordered layered perovskite electrode for symmetrical solid oxide fuel cells. J Mater Chem A 11(15):7995–8002. https://doi.org/10.1039/d2ta08892d
5. Zhao X, Yang X et al (2021) Tailoring an interstitial oxygen conducting electrode by in situ fabrication for quasi-symmetrical solid oxide fuel cells. Ionics 27(1):259–268. https://doi.org/10.1007/s11581-020-03790-4
6. Qin HC, Cheng Z et al (2023) Thermoelectrical comprehensive analysis and optimization of multi-stack solid oxide fuel cell system. Energy Conv Manag 291:18. https://doi.org/10.1016/j.enconman.2023.117297
7. Shen YF, Song Y et al (2022) Mo-doped $Ba_{0.5}Sr_{0.5}Co_{0.8}Fe_{0.2}O_{3-\delta}$ as a high-performance symmetric electrode for solid oxide fuel cells. J Alloy Compd 928:9. https://doi.org/10.1016/j.jallcom.2022.167029
8. Zhang M, Du ZH et al (2022) Progress of Perovskites as Electrodes for Symmetrical Solid Oxide Fuel Cells. ACS Appl Energ Mater 5(11):13081–13095. https://doi.org/10.1021/acsaem.2c02149
9. Zhang Y, Zhang X et al (2023) Pr-Doped $SrTi_{0.5}Mn_{0.5}O_{3-\delta}$ as an electrode material for a quasi-symmetrical solid oxide fuel cell using methane and propane fuel. Acs Appl Mater Interfaces 15(3):3974–3984. https://doi.org/10.1021/acsami.2c18530
10. Zhu K, Luo B et al (2022) Recent advances and prospects of symmetrical solid oxide fuel cells. Ceram Int 48(7):8972–8986. https://doi.org/10.1016/j.ceramint.2022.01.258
11. Zamudio-García J, Caizán-Juanarena L et al (2022) A review on recent advances and trends in symmetrical electrodes for solid oxide cells. J Power Sources 520:24. https://doi.org/10.1016/j.jpowsour.2021.230852
12. Zhang Y, Zhao HL et al (2023) Boosting the electrode reaction kinetics of SSOFCs by the synergistic effect of nanoparticle codecoration on both the cathode and anode. Chem Mat 35(2):499–510. https://doi.org/10.1021/acs.chemmater.2c02861
13. Ling YH, Li T et al (2021) Oxygen vacancies-rich iron-based perovskite-like electrodes for symmetrical solid oxide fuel cells. Ceram Int 47(9):12916–12925. https://doi.org/10.1016/j.ceramint.2021.01.154
14. Zhang JH, Lei LB et al (2021) A practical approach for identifying various polarization behaviors of redox-stable electrodes in symmetrical solid oxide fuel cells. Electrochim Acta 384:15. https://doi.org/10.1016/j.electacta.2021.138340
15. Beshiwork BA, Teketel BS et al (2022) Nanoengineering electrode for yttria-stabilized zirconia-based symmetrical solid oxide fuel cells to achieve superior output performance. Sep Purif Technol 295:14. https://doi.org/10.1016/j.seppur.2022.121174
16. Qian B, Wang S et al (2023) Cobalt-free double-perovskite oxide $Sr_2Ti_{0.9}FeNi_{0.1}O_6$ as a promising electrode for symmetric solid oxide electrolysis cells. J Eur Ceram Soc 43(16):7561–7572. https://doi.org/10.1016/j.jeurceramsoc.2023.08.006
17. Ding HP, Lin B et al (2008) High performance protonic ceramic membrane fuel cells (PCMFCs) with $Ba_{0.5}Sr_{0.5}Zn_{0.2}Fe_{0.8}O_{3-\delta}$ perovskite cathode. Electrochem Commun 10(9):1388–1391. https://doi.org/10.1016/j.elecom.2008.07.016
18. Shen LY, Du ZH et al (2021) Medium-entropy perovskites $Sr(Fe_\alpha Ti_\beta Co_\gamma Mn_\zeta)O_{3-\delta}$ as promising cathodes for intermediate temperature solid oxide fuel cell. Appl Catal B-Environ 295:10. https://doi.org/10.1016/j.apcatb.2021.120264
19. Zhang Y, Li JB et al (2023) CO_2-induced reconstruction for ORR-enhanced solid oxide fuel cell cathode. Chem Eng J 462:7. https://doi.org/10.1016/j.cej.2023.142216
20. Beshiwork BA, Wan XY et al (2024) A defective iron-based perovskite cathode for high-performance IT-SOFCs: tailoring the oxygen vacancies using Nb/Ta co-doping. J Energy Chem 88:306–316. https://doi.org/10.1016/j.jechem.2023.09.015
21. Gao JX, Zhang YJ et al (2021) Nitrogen-doped $Sr_2Fe_{1.5}Mo_{0.5}O_{6-\delta}$ perovskite as an efficient and stable catalyst for hydrogen evolution reaction. Mater Today Energy 20:7. https://doi.org/10.1016/j.mtener.2021.100695
22. Chen DJ, Wang FC et al (2012) Systematic evaluation of Co-free $LnBaFe_2O_{5+\delta}$ (Ln = Lanthanides or Y) oxides towards the application as cathodes for intermediate-temperature solid oxide fuel cells. Electrochim Acta 78:466–474. https://doi.org/10.1016/j.electacta.2012.06.073
23. Zhang BZ, Wan YH et al (2021) Tungsten-doped $PrBaFe_2O_{5+\delta}$ double perovskite as a high-performance electrode material for symmetrical solid oxide fuel cells. ACS Appl Energ Mater 4(8):8401–8409. https://doi.org/10.1021/acsaem.1c01618
24. Kim D, Son SJ et al (2021) $PrBaFe_2O_{5+\delta}$ promising electrode for redox-stable symmetrical proton-conducting solid oxide fuel cells. J Eur Ceram Soc 41(12):5939–5946. https://doi.org/10.1016/j.jeurceramsoc.2021.05.031
25. Son SJ, Kim D et al (2021) Investigation of oxygen ion transport and surface exchange properties of $PrBaFe_2O_{5+\delta}$. J Eur Ceram Soc 41(4):2691–2698. https://doi.org/10.1016/j.jeurceramsoc.2020.11.022
26. Zhang K, Ge L et al (2008) Synthesis, characterization and evaluation of cation-ordered $LnBaCo_2O_{5+\delta}$ as materials of oxygen permeation membranes and cathodes of SOFCs. Acta Mater 56(17):4876–4889. https://doi.org/10.1016/j.actamat.2008.06.004
27. Zhang Q, Wei T et al (2012) Electrochemical performance of double-perovskite Ba2MMoO6 (M=Fe Co, Mn, Ni) anode materials for solid oxide fuel cells. J Power Sour 198:59–65. https://doi.org/10.1016/j.jpowsour.2011.09.092
28. Jo S, Jeong HG et al (2021) Stability and activity controls of Cu nanoparticles for high-performance solid oxide fuel cells. Appl Catal B-Environ 285:7. https://doi.org/10.1016/j.apcatb.2020.119828
29. Zhang SW, Wan YH et al (2020) Bismuth doped $La_{0.75}Sr_{0.25}Cr_{0.5}Mn_{0.5}O_{3-\delta}$ perovskite as a novel redox-stable efficient anode for solid oxide fuel cells. J Mater Chem A 8(23):11553–11563. https://doi.org/10.1039/d0ta03328f
30. Chen FZ, Zhou DC et al (2023) Doping strategy on improving the overall cathodic performance of double perovskite $LnBaCo_2O_{5+\delta}$

(Ln=Pr, Gd) as potential SOFC cathode materials. J Materiomics 9(5):825–837. https://doi.org/10.1016/j.jmat.2023.02.004
31. He W, Wu XL et al (2017) A novel layered perovskite electrode for symmetrical solid oxide fuel cells: $PrBa(Fe_{0.8}Sc_{0.2})_2O_{5+\delta}$. J Power Sources 363:16–19. https://doi.org/10.1016/j.jpowsour.2017.07.059
32. Zhou J, Xu LY et al (2019) Layered perovskite $(PrBa)_{0.95}(Fe_{0.9}Mo_{0.1})_2O_{5+\delta}$ as electrode materials for high-performing symmetrical solid oxide electrolysis cells. Mater Lett 257:4. https://doi.org/10.1016/j.matlet.2019.126758
33. Liu CH, Wang F et al (2023) Ta-doped $PrBaFe_2O_5$ double perovskite as a high- performance electrode material for symmetrical solid oxide fuel cells. Int J Hydrog Energy 48(26):9812–9822. https://doi.org/10.1016/j.ijhydene.2022.11.237
34. Xiao GL, Liu Q et al (2012) Synthesis and characterization of Mo-doped $SrFeO_{3-\delta}$ as cathode materials for solid oxide fuel cells. J Power Sources 202:63–69. https://doi.org/10.1016/j.jpowsour.2011.11.021
35. Jiang SS, Sunarso J et al (2015) Cobalt-free $SrNb_xFe_{1-x}O_{3-\delta}$ (x=0.05, 0.1 and 0.2) perovskite cathodes for intermediate temperature solid oxide fuel cells. J Power Sources 298:209–216. https://doi.org/10.1016/j.jpowsour.2015.08.063
36. Wang SB, Xu JS et al (2021) Cobalt-free perovskite cathode $BaFe_{0.9}Nb_{0.1}O_{3-\delta}$ for intermediate-temperature solid oxide fuel cell. J Alloy Compd 872:10. https://doi.org/10.1016/j.jallcom.2021.159701
37. Li H, Wei B et al (2020) Novel cobalt-free layered perovskite $LaBaFe_{2-x}Nb_xO_{6-\delta}$ (x=0-0.1) as cathode for solid oxide fuel cells. J Power Sources 453:10. https://doi.org/10.1016/j.jpowsour.2020.227875
38. Wang S, Qian B et al (2021) High catalytic activity of Fe-based perovskite fuel electrode for direct CO_2 electroreduction in SOECs. J Alloy Compd 888:10. https://doi.org/10.1016/j.jallcom.2021.161573
39. Lu CL, Niu BB et al (2020) Efficient symmetrical electrodes of $PrBaFe_{2-x}Co_xO_{5+\delta}$ (x=0, 0.2,0.4) for solid oxide fuel cells and solid oxide electrolysis cells. Electrochim Acta 358:12. https://doi.org/10.1016/j.electacta.2020.136916
40. Lü SQ, Zhu YZ et al (2022) A-site deficient Fe-based double perovskite oxides $Pr_xBaFe_2O_{5+\delta}$ as cathodes for solid oxide fuel cells. J Alloy Compd 911:12. https://doi.org/10.1016/j.jallcom.2022.165002
41. Gao JT, Liu YY et al (2023) Cobalt-free fluorine doped $Bi_{0.7}Sr_{0.3}FeO_{3-\delta}$ oxides for energetic cathodes of low-temperature solid oxide fuel cells. Chem Eng J 452:11. https://doi.org/10.1016/j.cej.2022.139584
42. Qiu P, Li C et al (2023) Materials of solid oxide electrolysis cells for H_2O and CO_2 electrolysis: a review. J Adv Ceram 12(8):1463–1510. https://doi.org/10.26599/jac.2023.9220767
43. Liu SB, Sun C et al (2020) A high-performance Ruddlesden-Popper perovskite for bifunctional oxygen electrocatalysis. ACS Catal 10(22):13437–13444. https://doi.org/10.1021/acscatal.0c02838
44. Mao XB, Wang WB et al (2015) A novel cobalt-free double-perovskite $NdBaFe_{1.9}Nb_{0.1}O_{5+\delta}$ cathode material for proton-conducting IT-SOFC. Ceram Int 41(8):10276–10280. https://doi.org/10.1016/j.ceramint.2015.03.326
45. Wang SZ, Fin FJ et al (2017) Stability, compatibility and performance improvement of $SrCo_{0.8}Fe_{0.1}Nb_{0.1}O_{3+\delta}$ perovskite as a cathode for intermediate-temperature solid oxide fuel cells. Int J Hydrog Energy 42(7):4465–4477. https://doi.org/10.1016/j.ijhydene.2016.11.015
46. Lee J, Bark H et al (2023) Size-selective ionic crosslinking provides stretchable mixed ionic–electronic conductors. Angewandte Chemie Int Edition 62:06520. https://doi.org/10.1002/ange.202306994
47. Han X, Ling YH et al (2023) Utilizing high entropy effects for developing chromium-tolerance cobalt-free cathode for solid oxide fuel cells. Adv Funct Mater 33(43):9. https://doi.org/10.1002/adfm.202304728
48. Bian LZ, Duan CC et al (2018) Electrochemical performance and stability of $La_{0.5}Sr_{0.5}Fe_{0.9}Nb_{0.1}O_{3-\delta}$ symmetric electrode for solid oxide fuel cells. J Power Sources 399:398–405. https://doi.org/10.1016/j.jpowsour.2018.07.119
49. Cao YX, Zhu ZW et al (2020) Development of tungsten stabilized $SrFe_{0.8}W_{0.2}O_{3-\delta}$ material as novel symmetrical electrode for solid oxide fuel cells. J Power Sources 455:11. https://doi.org/10.1016/j.jpowsour.2020.227951
50. Niu BB, Jin FJ et al (2018) Performance of double perovskite symmetrical electrode materials $Sr_2TiFe_{1-x}MoO_{6-x}$ ($x = 0.1, 0.2$) for solid oxide fuel cells. Electrochim Acta 263:217–227. https://doi.org/10.1016/j.electacta.2018.01.062
51. Lü SQ, Meng XW et al (2012) Performances of $SmBaCoCuO_{5+\delta}$-$Ce_{0.9}Gd_{0.1}O_{1.95}$ composite cathodes for intermediate-temperature solid oxide fuel cells. Int J Hydrog Energy 37(23):18319–18325. https://doi.org/10.1016/j.ijhydene.2012.09.043
52. Li GD, Gou YJ et al (2021) Enhanced electrochemical performance of the Fe-based layered perovskite oxygen electrode for reversible solid oxide cells. Acs Appl Mater Interfaces 13(29):34282–34291. https://doi.org/10.1021/acsami.1c08010
53. Liu B, Jia LC et al (2020) A novel $PrBaCo_2O_{5+\delta}$-$BaZr_{0.1}Ce_{0.7}Y_{0.1}Yb_{0.1}O_{3+\delta}$ composite cathode for proton-conducting solid oxide fuel cells. Compos Pt B-Eng 191:7. https://doi.org/10.1016/j.compositesb.2020.107936
54. Zhang Y, Zhang BZ et al (2021) Electrochemical performance and structural durability of Mg-doped $SmBaMn_2O_{5+\delta}$ layered perovskite electrode for symmetrical solid oxide fuel cell. Catal Today 364:80–88. https://doi.org/10.1016/j.cattod.2020.05.057
55. Tian D, Lin B et al (2016) Enhanced performance of symmetrical solid oxide fuel cells using a doped ceria buffer layer. Electrochim Acta 208:318–324. https://doi.org/10.1016/j.electacta.2016.04.189
56. Luo XY, Yang Y et al (2018) Reduced-temperature redox-stable LSM as a novel symmetrical electrode material for SOFCs. Electrochim Acta 260:121–128. https://doi.org/10.1016/j.electacta.2017.11.071
57. Dos Santos-Gómez L, Porras-Vázquez JM et al (2020) Investigation of PO43- oxyanion-doping on the properties of $CaFe_{0.4}Ti_{0.6}O_{3-\delta}$ for potential application as symmetrical electrodes for SOFCs. J Alloy Compd 835:8. https://doi.org/10.1016/j.jallcom.2020.155437
58. Li M, Zheng MH et al (2017) Improving electrochemical performance of lanthanum strontium ferrite by decorating instead of doping cobaltite. Electrochim Acta 230:196–203. https://doi.org/10.1016/j.electacta.2017.02.014
59. Zhang Y, Shen LY et al (2022) Enhanced oxygen reduction kinetics of IT-SOFC cathode with $PrBaCo_2O_{5+\delta}$/$Gd_{0.1}Ce_{1.9}O_{2-\delta}$ coherent interface. J Mater Chem A 10(7):3495–3505. https://doi.org/10.1039/d1ta09615j
60. Wang S, Jiang HG et al (2020) Mo-doped $La_{0.6}Sr_{0.4}FeO_{3-\delta}$ as an efficient fuel electrode for direct electrolysis of CO2 in solid oxide electrolysis cells. Electrochim Acta 337:11. https://doi.org/10.1016/j.electacta.2020.135794